Joint Range-Doppler-Angle Estimation for Intelligent Tracking of Moving Aerial Targets

Liangtian Wan, *Member, IEEE*, Xiangjie Kong, *Senior Member, IEEE*, and Feng Xia, *Senior Member, IEEE*

***Abstract*—In the new era of integrated computing with intelligent devices and system, moving aerial targets can be tracked flexibly. The estimation performance of traditional matched filter-based methods would deteriorate dramatically for multiple targets tracking, since the weak target is masked by the strong target or the strong sidelobes. In order to solve the problems mentioned above, this paper aims at developing a joint range-Doppler-angle estimation solution for an intelligent tracking system with a commercial frequency modulation radio station (noncooperative illuminator of opportunity) and a uniform linear array. First, a gridless sparse method is proposed for simultaneous angle-range-Doppler estimation with atomic norm minimization. Based on the integrated computing, multiple workstations or servers of the data process center in the intelligent tracking system can cooperate with each other to accelerate the data process. Then a suboptimal method, which estimates three parameters in a sequential way, is proposed based on grid sparse method. The range-Doppler of each target is iteratively estimated by exploiting the joint sparsity in multiple surveillance antennas. A simple beamforming method is used to estimate the angles in turn by exploiting the angle information in the joint sparse coefficients. Simulation result and real test show that the proposed solution can effectively detect weak targets in an iterative manner.**

***Index Terms*—Atomic norm, compressed sensing, intelligent computing, Internet of Things (IoT), optimization, target tracking.**

I. Introduction

DRIVEN by the proliferation of more sophisticated smart-phone and wireless communication techniques, the scale of Internet of Things (IoT) devices will continue to grow at an exponential pace [1]. Integrated computing provides a promising solution to the industry for building the IoT systems based on cloud and fog computing [2], [3]. Intelligent devices and intelligent systems are two major components in the new era of integrated computing [4]. Radar systems which are one kind of intelligent systems [5], are useful tools for detecting valuable information from environment, and there have been various applications in military and industry [6]–[8]. In the data process center of the radar system, tremendous data is needed to be processed in real time. It is not possible for single workstation or server process the whole data, thus various workstations or servers are needed to cooperate with each other. Integrated computing is a promising way to solve this problem. Many devices of data process center are connected in an intelligent way based on an identical software platform and its associated physical system of integrated computing. The efficiency of the data process center can be improved dramatically.

Passive bistatic radar (PBR) system is known as a variant of traditional radar systems that can date back to more than decades ago [9]. A PBR system has some benefits that an active radar does not have. First, a PBR system can exploit " noncooperative illuminators of opportunity" as their sources of radar transmission and do not need a dedicated transmitter. Therefore, it has low cost and can be covert, and becomes attractive for a broad range of applications. Second, the PBR system has the ability to operating in a wide frequency band without interference with existing wireless systems. Typical illuminators of opportunity includes television [10] and radio broadcast stations [11], cellphone base stations [12], digital video broadcast [13], etc. Finally, The bistatic or multistatic configuration enables it to obtain spatial diversity to improve the target detection and classification performance [14], [15].

A typical PBR system exploits a single noncooperative illuminators of opportunity, referred as a transmitter antenna. The reference antenna is steered toward the transmitter to collect a direct path signal (i.e., reference signal), while a surveillance antenna is used to measure a potential target echo (surveillance signal) [6], [7], [11]. The reference signal is crucial since it can be used to eliminate interference echoes in surveillance signal, e.g., direct signals, clutters, and multipath signals [11]. Then the potential targets can be detected by conducting delay-Doppler cross-correlation operation (matched filter) between reference and surveillance signals [6], [11]. However, the detected performance would be degraded significantly since the reference signal is contaminated with inevitable noise. In [16], several new signal detectors have been proposed by exploiting the noisy nature of reference signal. The performance of the matched filter detector with the noisy reference signal has been analyzed in [17]. Other state-of-the-art approaches are to exploit the passive multi-input multioutput (MIMO) radar network to improve target detection and estimation performance [15]. The interplay between

Manuscript received September 15, 2017; revised December 6, 2017; accepted December 19, 2017. Date of publication December 28, 2017; date of current version June 8, 2018. This work was supported in part by the School of Electrical and Electronic Engineering, Nanyang Technological University, Singapore, in part by the National Natural Science Foundation of China under Grant 61572106, and in part by the Fundamental Research Funds for the Central Universities under Grant DUT17RC(3)029. *(Corresponding author: Feng Xia.)*

The authors are with the Key Laboratory for Ubiquitous Network and Service Software of Liaoning Province, School of Software, Dalian University of Technology, Dalian 116620, China (e-mail: f.xia@ieee.org).

Digital Object Identifier 10.1109/JIOT.2017.2787785

the noise in different receivers has been extensively studied in [15]. The correlations of reference and surveillance signals across receivers are used to extract valuable information from multiple receivers [15], [18].

However, some issues still exist in the works mentioned above. First, the multipath signals or clutters in reference signal are not always paid enough attention. The detect performance would be degraded without considering strong multipath propagations or clutters and this problem is even worse in the approaches based on matched filter [11]. However, there are few literatures about the cancellation of multipath signals or clutters in the reference signal. In order to remove their effect, the structure of general side-lobe canceller [19] is proposed to realize the adaptive beamforming in the reference channel [20] by an adaptive antenna array, e.g., uniform circular array.

It is often assumed that the surveillance antenna only receives the target echo without the direct path from the transmitter. In particular, the strength of direct-path may much stronger than that of target echo, an empirical value pointed in [20] is about 70 dB. The directional antennas can be used to mitigate this dilemma. However, this direct path interference may still exist in the surveillance signal. Then a beamforming method has been used for direct path interference suppression by setting null toward the direction-of-arrivals (DOAs) of direct path and multipath signals or clutters based on a uniform circular array [20]. In [21], the reference antenna is replaced by a uniform linear array (ULA), and the constant modulus algorithm approach has been used by synthesising an equivalent pattern in which zeros are set at given DOAs corresponding to the multipath signals. However, the mitigation is limited by the array aperture which dictates the null depth. Then the direct path is considered in the surveillance signal, and the range-Doppler have been estimated based on expectation-maximization principle [22]. In addition, the angles of targets are the parameters of interest as well. So far, the methods mentioned above cannot estimate angle-range-Doppler jointly in passive sensing system, e.g., PBR, passive multistatic radar, and passive MIMO radar network systems.

The recently developed compressed sensing theory and methods can achieve acquisition of information in a huge volume of data only with a small number of measurement samples [23], [24]. Despite the tremendous benefits of compressed sensing on DOA estimation, many literatures have focused on parameter discretization with a compact dictionary based on grid sparse methods [25]. However, the DOAs are specified in a continuous domain and the estimation is approximately achieved in a discrete domain spanned by a finite set of grid points. Thus the grid sparse method suffers from basis mismatch problem [26], i.e., the true parameters do not fall onto the finite grid, which leads to inaccurate DOA estimation. Instead the gridless sparse method has been proposed with atomic norm minimization for continuous compressed sensing (CCS) [27]–[29], which completely solve the basis mismatch problem [28]. For DOA estimation with CCS, a novel (nonconvex) sparse metric is proposed that promotes sparsity to a greater extent than the atomic norm [30]. The estimation performances of state-of-the-art compressed sensing methods are much better than the traditional subspace methods. However, the computational complexity of these methods is much larger than that of the subspace-based methods. Since the objective of the intelligent tracking system is to track the targets in real time, the computational intensive methods such as the compressed sensing-based methods cannot be used.

In this paper, we make the following contributions.

1) A simultaneous angle-range-Doppler estimation algorithm is proposed with atomic norm minimization where the direct path is known as a prior, since angle-range-Doppler parameters of targets are sparse in frequency domain via 3-D discrete Fourier transform. Due to the tremendous dimension of sensing matrix, this method is almost impossible to implement in practical scenario because of the limitation of hardware resource. However, based on the integrated computing, multiple workstations or servers of the data process center can cooperate with each other, this method can be implement in the real system in the future.
2) The joint sparsity in multiple channels are exploited when the direct path is known. The range-Doppler of each target is estimated iteratively using the joint sparse counterpart of multiple orthogonal matching pursuit (M-OMP) [31], [32]. The angle information is contained in the coefficients of the joint sparse recovery problem that has been solved in range-Doppler estimation. As a result, a simple beamforming method can be adopted to estimate this parameter in turn.
3) The subspace methods, which have much lower computational complexity compared with the grid sparse and gridless sparse method proposed recently [30], are adopted for DOA estimation of direct path when the direct path is unknown. Then the direct path can be estimated by using a least squares method given the array data. Finally, numerical simulations and real test are carried out to verify the effectiveness of the proposed algorithms.

Some important notations used in this paper are summarized in Table I. The rest of this paper is organized as follows. The system architecture and signal model are elaborated in Section II. The disturbance cancellation and matched filter technique is reviewed in Section III. The angle-range-Doppler estimation algorithms based on compressed sensing are proposed in Section IV. The simulation results and real test are shown in Section V. The conclusions are drawn in Section VI.

II. Problem Statement

As depicted in Fig. 1, an intelligent tracking system exploits a single noncooperative illuminator of opportunity, referred as a transmitter antenna. When a target is presented in the surveillance space of interest, it reflects the transmitted signal that contains information of itself. Thus, a surveillance array can be implemented to acquire the reflected target echo for processing to infer the target information. Furthermore, while the

TABLE I
SUMMARY OF NOTATION

Symbol	Definition
$d(t)$	direct signal
τ_{ci}	the delay (with respect to the direct signal) of the ith ground scatterer
c_i	the complex amplitude
N_C	the total number of such scatterers
a_m	the complex amplitude of the mth target
τ_m	the delay (with respect to the direct signal) of the mth target
f_{TDm}	the Doppler frequency of the mth target
N_T	the number of targets
$n(t)$	the thermal noise
ΔR_{bis}	The relative bistatic range between a backscattered echo and the direct signal
R_{bis}	the distance that the echo travels
B	the distance between the transmitter and the receiver
c	the speed of light
$s(t,l)$	the signal received by the lth antenna at time t
$n(t,l)$	the measurement noise
f_{DA}	the angle frequency of the direct path
f_{CAi}	the ith clutter
f_{TAm}	the mth target
θ_{DA}	the angles of the direct path
λ	the wavelength
τ_{Ci}	the bistatic delay of the ith clutter
τ_m	the bistatic delay of the mth target
f_{TDm}	the Doppler frequency of the mth target
$\mathbf{x} \in \mathbb{C}^N$	called K-sparse if all but at most a number of $K \ll N$ entries are zero
$y \in \mathbb{C}^M$	the measurement vector
$\mathbf{A} \in \mathbb{C}^{M \times N}$	the dictionary
$\mathbf{D}$	each atom/column is a delayed or Doppler shifted version of the direct signal
$s_T(t)$	the target echoes
$\mathbf{\Phi}$	$L_T L_A \times L_T^2 L_A$ dictionary
$\mathbf{a}(\theta_m)$	a function of $\theta_m \in \mathcal{D} \subset \mathbb{R}^p$ of interest
$s_{ref}(t)$	the reference signal

surveillance array acquires the target echo, it will inevitably receive signals from other sources such as the direct path from the transmitter antenna as well as multipath and clutter echoes from ground and surrounding buildings. The received data can be processed in the data process center, and the integrating computing provide an identical platform with various devices.

Remark 1: The radar system used throughout this paper is slightly different from the one presented in [11] and a frequency modulation radio station is used as the transmitter antenna. Instead of using a single surveillance antenna, we implement an antenna array consisting of multiple surveillance antennas. It follows from the knowledge of array processing that the direct signal can be estimated by beamforming (i.e., by steering the outputs of the antenna array toward the direction of the transmitter antenna). Therefore, the estimate of the direct signal does play the role of a virtual reference antenna, instead of physical implementation of an additional reference antenna. Note that our system model is notably different from those in prior delay-Doppler estimation works [34] and angle-Doppler-range estimation works for MIMO radar [35]–[37].

In the remaining of this section, the problem formulation of the PBR system is stated at first, then the basic concept about grid sparse and gridless sparse models are given.

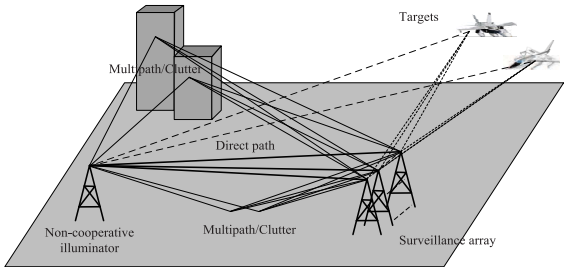

Fig. 1. Intelligent tracking system: PBR system.

A. Observation Model

Given a direct signal $d(t)$, a complex envelope of the total signal in the surveillance antenna is given by

$$s(t) = d(t) + \sum_{i=1}^{N_C} c_i d(t - \tau_{ci}) + \sum_{m=1}^{N_T} a_m d(t - \tau_m) e^{j2\pi f_{TDm} t} + n(t). \quad (1)$$

$0 \le t < T_0$, where $d(t)$ is the direct signal, τ_{ci} denotes the delay (with respect to the direct signal) of the ith ground scatterer, c_i is the complex amplitude, and N_C is the total number of such scatterers. The third term on the right-hand side denotes the target echoes and a_m, τ_m, and f_{TDm} denote the complex amplitude, the delay (with respect to the direct signal), and the Doppler frequency of the mth target, respectively. N_T is the number of targets, and $n(t)$ denotes the thermal noise. The relative bistatic range between a backscattered echo and the direct signal is $\Delta R_{\text{bis}} = R_{\text{bis}} - B = c\tau$, where R_{bis} is the distance that the echo travels, B is the baseline, i.e., the distance between the transmitter and the receiver, and c is the speed of light.

Consider the case that multiple antennas forms an antenna array. The transmitted frequency modulation signal is narrowband, and the distance from the array to the targets is much greater than the array aperture in practice. It follows from [39] and [40] that, for every target echo (as well as the direct signal), the time delay between adjacent surveillance antennas can be expressed as a phase shift. Thus, when the surveillance antennas form the ULA with adjacent antennas spaced by δ_A, the signal received by the ULA can be written as

$$s(t,l) = d(t)e^{j2\pi f_{DA} l} + \sum_{i=1}^{N_C} c_i d(t - \tau_{ci}) e^{j2\pi f_{CAi} l} + \sum_{m=1}^{N_T} a_m d(t - \tau_m) e^{j2\pi f_{TDm} t} e^{j2\pi f_{TAm} l} + n(t), \quad 0 \le t < T_0; 0 \le l < L_A \quad (2)$$

where $s(t,l)$ denotes the signal received by the lth antenna at time t, $d(t)$ is the direct path, and $n(t,l)$ is the measurement noise. $f_{DA} = (\delta_A/\lambda)\cos\theta_{DA}$, $f_{CAi} = (\delta_A/\lambda)\cos\theta_{CAi}$, and $f_{TAm} = (\delta_A/\lambda)\cos\theta_{TAm}$ denote the angle frequency of the direct path, the ith clutter and the mth target, respectively, where θ_{DA}, θ_{CAi}, and θ_{TAm} denote the angles of the direct path, the ith clutter and the mth target, respectively, and λ is the

wavelength. τ_{Ci} and τ_m are the bistatic delay of the ith clutter and the mth target, respectively. f_{TDm} is the Doppler frequency of the mth target. Given $s(t, l)$, the goal is to estimate the target parameters τ_m, f_{TDm}, and f_{TAm}.

B. Parameter Estimation Based on Grid-Based Model

A signal $\mathbf{x} \in \mathbb{C}^N$ is called K-sparse if all but at most a number of $K \ll N$ entries are zero. In the PBR system, the number of targets is usually limited thus yielding sparsity. Rather than observing directly the original sparse signal $\mathbf{x}$, a number of M, $K < M \ll N$, linear measurements are acquired in compressed sensing as

$$\mathbf{y} = \mathbf{A}\mathbf{x} \tag{3}$$

where $y \in \mathbb{C}^M$ is the measurement vector and $\mathbf{A} \in \mathbb{C}^{M\times N}$ denotes the dictionary. By accounting for the signal sparsity, naturally, we want to find the sparsest solution by solving the combinational optimization problem

$$\min\|\mathbf{x}\|_0, \quad \text{subject to } \mathbf{y} = \mathbf{A}\mathbf{x} \tag{4}$$

where $\|\mathbf{x}\|_0$ denotes the pseudo l_0 norm which counts the number of nonzero entries of $\mathbf{x}$. When some measurement vectors share the same support, we would recover a joint-sparse signal from multiple measurement vectors. Using (3), we can write

$$\mathbf{Y} \coloneqq \left[\mathbf{y}(1), \ldots, \mathbf{y}(\kappa)\right] = \mathbf{A}\mathbf{X} \tag{5}$$

where $\mathbf{X} \coloneqq [\mathbf{x}(1), \ldots, \mathbf{x}(\kappa)]$ is a sparse matrix, and only K rows are nonzero. Such a matrix is called jointly K-sparse. Thus the multiple measurement vectors problem is often solved by solving

$$\min\|\mathbf{X}\|_{g,h}, \quad \text{subject to} \quad \mathbf{Y} = \mathbf{A}\mathbf{X} \tag{6}$$

for some integers g and h, where $\|\mathbf{X}\|_{g,h}$ is defined as

$$\|\mathbf{X}\|_{g,h} = \left[\sum_{\bar{j}=1}^{N}\left(\sum_{\bar{i}=1}^{\kappa}\left|X[\bar{j}, \bar{i}]\right|^g\right)^{h/g}\right]^{1/h}. \tag{7}$$

In this paper, $g = 2$ and $h = 0$ are used. Since the dictionary is a finite set of grid points, we can recover a joint sparse $\mathbf{X}$ from $\mathbf{Y}$ using grid sparse-based methods.

III. Disturbance Cancellation and Target Localization

According to the well known bistatic radar equation (see [38]), direct signal and clutter are much stronger than target echoes. Therefore, disturbance cancellation is the first and a very important task in PBR signal processing. So far several cancellation techniques have been proposed in [41]–[43]. We revisit the extensive cancellation algorithm in [43] by using a least squares approach. In the algorithm, a dictionary/matrix $\mathbf{D}$ is constructed, where each atom/column is a delayed or Doppler shifted version of the direct signal that corresponds to one potential source of disturbance. It follows that the range space of $\mathbf{D}$ defines the space of disturbance. Given a surveillance signal $s(t)$, disturbance cancellation is thus obtained by projecting it onto the orthogonal subspace of the range space of $\mathbf{D}$. The projection is regraded as the target echoes (subject to noise). Therefore, the main task of the algorithm is to select the locations of the potential sources of disturbance. Based on the aforementioned modeling of the multipath and clutter, the first several range bins with zero (or very small) Doppler can be selected to form $\mathbf{D}$ and the same procedure can be achieved for all the surveillance antennas to cancel out the disturbance. This is the reason that the modeling of the nearfield ground echoes is trivial since they can be canceled out using this method without using their angle information. The computational complexity of the disturbance cancellation is large, the integrating computing will provide a faster computation way in the future.

After disturbance cancellation, the remaining task is target detection and localization. A common approach is matched filter that evaluates the cross-correlation function (CCF) between the obtained target echoes and the reference signal. Consider range-Doppler estimation as an example, the delay-Doppler CCF is defined as

$$\xi(\tau, f_D) = \int_0^{T_0} s_T(t) \cdot s_{ref}^*(t) \cdot e^{-j2\pi f_D t} dt \tag{8}$$

where $s_T(t)$ denotes the target echoes. If $s_T(t)$ contains only a single target echo with parameters (τ, f_D), then the CCF achieves the maximum at (τ, f_D). But if $s_T(t)$ consists of several target echoes, then weak targets can be masked by sidelobes of strong targets due to the aforementioned self-ambiguity of frequency modulation signal. Moreover, if some strong disturbance has not been canceled out and remains in $s_T(t)$, then targets of interest can be masked by the sidelobes of disturbance.

IV. Angler-Range-Doppler Estimation by Exploiting Signal Sparsity

In this section, we discuss the feasibility for gridless sparse method for simultaneous angular-range-Doppler estimation in PBR system, since it can overcome the basis mismatch problem which leads to high estimation accuracy compared with the grid sparse method. However, due to the tremendous computational complexity of the gridless sparse method in this 3-D sparse recovery case, we present a grid sparse method for angular-range-Doppler estimation in PBR exploiting signal sparsity in the following.

A. Gridless Sparse Method for Simultaneous Angle-Range-Doppler Estimation

With the disturbance cancellation, we can do cancellation for each antenna and retrieve the target echoes given by

$$s(t, l) = \sum_{m=1}^{N_T} a_m d(t - \tau_m) e^{j2\pi f_{TDm} t} e^{j2\pi f_{TAm} l} + n(t), \quad 0 \le t < T_0; 0 \le l < L_A. \tag{9}$$

Based on the discrete Fourier transform, the delay of direct path $d(t - \tau_m)$ can be written as

$$d(p - \tau_m) = \frac{1}{L}\sum_{k=-N}^{N} e^{i2\pi \frac{pk}{L}} \hat{D}_k e^{-i2\pi k \tau_m}. \tag{10}$$

Then (9) can be reformulated as

$$s(p,l) = \frac{1}{L}\sum_{k=-N}^{N} e^{i2\pi\frac{pk}{L}}\hat{D}_k \sum_{m=1}^{N_T} a_m e^{-i2\pi(k\tau_m + pf_{TDm} + lf_{TAm})} + n(p), \quad p=-N_p,\ldots,N_p;\ l=-N_A,\ldots,N_A \tag{11}$$

where the snapshot number is $L_T = 2N_p + 1$ and the number of antennas is $L_A = 2N_A + 1$. We can rewrite (11) in matrix form as

$$\mathbf{y} = \mathbf{\Phi}\mathbf{z}, \quad \mathbf{z} = \sum_{m=1}^{N_T} a_m b(\tau_m, f_{TDm}, f_{TAm}) \tag{12}$$

where

$$b_{k,p,l}(\tau_m, f_{TDm}, f_{TAm}) = e^{-i2\pi(k\tau_m + pf_{TDm} + lf_{TAm})}. \tag{13}$$

In fact, $b_{k,p,l}(\tau_m, f_{TDm}, f_{TAm})$ can be regarded as a third order sparse tensor, since only a few points in the cube are nonzero based on the inverse 3-D discrete Fourier transform. $\mathbf{\Phi}$ is an $L_T L_A \times L_T^2 L_A$ matrix which can be expressed as

$$\mathbf{\Phi}_{(k,l)\times(k',p',l')} = \begin{cases} \frac{1}{L_T} e^{i2\pi\frac{k'k}{L}}\hat{D}_{k'}, & \text{if } p'+k=0 \\ & \text{and } l'+l=0 \\ 0, & \text{otherwise.} \end{cases} \tag{14}$$

The detail on the derivation of $\mathbf{\Phi}$ can be found in the Appendix.

The atomic norm is a more general version of L_1 norm and the nuclear norm of matrices, and it was first introduced in [27]. Let $\mathcal{A}$ be a compact set, which collects all the atoms. The convex null, conv($\mathcal{A}$), is centrally symmetric, and the origin is contained as an interior point [30]. Then the atomic norm is the gauge function of conv($\mathcal{A}$)

$$\|\mathbf{y}\|_{\mathcal{A}} \triangleq \{t>0 : \mathbf{y} \in t\,\mathrm{conv}(\mathcal{A})\} = \inf\left\{\sum_k c_k : y = \sum_k c_k \mathbf{a}_k,\ c_k \geqslant 0,\ \mathbf{a}_k \in \mathcal{A}\right\}. \tag{15}$$

According to the definition of atomic norm in [28], we can estimate angular-range-Doppler simultaneously by using the atomic norm minimization

$$\min_{\mathbf{z}} \|\mathbf{z}\|_{\mathcal{A}}, \ \text{subject to } \mathbf{y} = \mathbf{\Phi}\mathbf{z}. \tag{16}$$

This paper is similar with the related work about MIMO radar [44]. The proposed algorithm and the algorithm in [44] can completely resolve the grid mismatch problem of existing compressed sensing method based on the continuous parameter estimation. The theoretical performance can be guaranteed to reveal how many targets can be estimated and what is the achievable resolution [44]. However, it should be noted that the computation of estimation is quite expensive due to the huge sensing matrix $\mathbf{\Phi}$. In fact, its dimension is $L_T L_A \times L_T^2 L_A$ and we need 1 s of data when we do CCF [38]. The sampling frequency is 400 kHz, the snapshot number L_T is equal to 4×10^5. Assume that the number of antennas L_A is 8. Then the dimension of $\mathbf{\Phi}$ is $(3.2\times10^6)\times(1.28\times10^{12})$. This atomic norm minimization problem of (16) cannot be solved in practice. However, based on the integrated computing, multiple workstations or servers of the data process center can cooperate with each other, this method can be implement in the real system in the future. Thus grid sparse method has to be taken into consideration.

Algorithm 1 M-OMP

Input: residual $\mathbf{R}_0 = \mathbf{Y}$ and subset $\mathbf{Z}_0 = \emptyset$,
Output: the support of $\mathbf{X}$.
At the vth iteration:
a). match: choose the atom $\mathbf{a}_{\bar{m}_v}$ which satisfies $\mathbf{a}_{\bar{m}_v} = \mathrm{argmax}_{\mathbf{a}_{\bar{m}}}\|\mathbf{z}_{\bar{m}}\|_1$, where $\mathbf{z}_{\bar{m}} = \mathbf{R}_{v-1}^T\mathbf{a}_{\bar{m}}$;
b). identify: let $\mathbf{Z}_v = [\mathbf{Z}_{v-1}, \mathbf{a}_{\bar{m}_v}]$;
c). update: $\mathbf{X}^* = \mathrm{argmin}_{\mathbf{X}}\|\mathbf{Z}_v\mathbf{X} - \mathbf{Y}\|_F^2$, $\mathbf{w}_v = \mathbf{Z}_v\mathbf{X}^*$;
Set $\mathbf{R}_v = \mathbf{Y} - \mathbf{w}_v$.

B. Grid Sparse Method for Angle-Range-Doppler Estimation With Known Direct Path

Given a direct path $d(t)$ with the cancellation, target echoes can be rewritten as

$$\mathbf{Y} = \sum_{m=1}^{N_T} \mathbf{x}_m \mathbf{a}(\theta_m) \tag{17}$$

where $\mathbf{a}(\theta_m)$ is a function of $\theta_m \in \mathcal{D} \subset \mathbb{R}^p$ of interest. Given the $L_A \times L_T$ data matrix $\mathbf{Y}$, the goal is to estimate the parameters $\theta_m, m = 1,\ldots,N_T$. To do this, we form a grid $\theta_{\bar{m}}, \bar{m} = 1,\ldots,\bar{N}_T$ in the parameter domain $\mathcal{D}$. Assume that $\{\theta_m\}$ lie on (practically, close to) this grid. The data model (17) can be written as the following linear system of equations:

$$\mathbf{Y} = \sum_{\bar{m}=1}^{\bar{N}_A} \mathbf{x}_k \mathbf{a}\big(\widetilde{\theta}_{\bar{m}}\big) = \mathbf{A}\mathbf{X} \tag{18}$$

where $\mathbf{A}$ is composed of the atoms $\mathbf{a}(\widetilde{\theta}_{\bar{m}})$, and the parameters θ_m of interest are encoded in the support of the matrix $\mathbf{X}$ with sparse rows. If $\mathbf{X}$ cam be solved given $\mathbf{Y}$, then the parameters can be estimated. Therefore, the sparse parameter estimation problem in (17) can be converted to a multiple measurement vector optimization in compressed sensing as follows:

$$\min_{\mathbf{X}} \ \|\mathbf{X}\|_{2,0} \quad \text{subject to } \ \mathbf{Y} = \mathbf{A}\big(\widetilde{\tau}_{\bar{m}_1}, \widetilde{f}_{\bar{m}_2}\big)\mathbf{X}. \tag{19}$$

In the first stage of the algorithm, the range-Doppler of the target is estimated. we have L_A antennas that share the same range-Doppler information. The joint sparsity can be imposed in the L_A channels and the range-Doppler can be estimated by using the joint sparse M-OMP [31], [32]. The entire algorithm procedure can be summarized in Algorithm 1, in which $\mathbf{a}_{\bar{m}}$ stands for $\mathbf{a}(\widetilde{\theta}_{\bar{m}})$.

We choose the atom in the dictionary, and then calculate the product of the residual error and each atom (line a). The atom that make the product achieve the maximum value is selected (line b). Then we use the least squares to calculate $\mathbf{X}^*$, and the residual value can be calculated based on the product of the matrix constructed by the selected atoms and $\mathbf{X}^*$ (line c). Then the residual error can be calculated. We repeat this procedure until the stopping criterion is satisfied.

In order to estimate the delay-Doppler (range-Doppler), a grid $\{(\widetilde{\tau}_{\bar{m}_1}, \widetilde{f}_{\bar{m}_2})\}$ is formed in the delay-Doppler plane of interest. For each grid cell $(\widetilde{\tau}_{\bar{m}_1}, \widetilde{f}_{\bar{m}_2})$, an atom $\mathbf{a}_{\bar{m}_1,\bar{m}_2}$ is obtained by $\mathbf{a}_{\bar{m}_1,\bar{m}_2}(t) = d(t - \widetilde{\tau}_{\bar{m}_1})e^{j2\pi \widetilde{f}_{\bar{m}_2} t}$. As a result, the range-Doppler estimation problem can be modeled as a sparse recovery problem. Being different from the standard sparse recovery, a subset of the supports of a sparse signal is known or approximately known. For example, the atom at $(\tau, f) = (0, 0)$ actually refers to the direct signal and thus it should be included in the support of the sparse signal. Recall the disturbance cancellation in the previous section. The first range cells/bins are potential sources of ground echoes and also can be included in the support. Therefore, we have partially known support in the sparse recovery problem that can be taken into account.

Then M-OMP can be applied to solve the sparse recovery problem. To incorporate the aforementioned support information, M-OMP is initialized with $\mathbf{Z}_0$ consisting of the indices of disturbance (the direct signal and the ground echoes) and $\mathbf{Y}$ being the residual of disturbance cancellation using the least squares method. This is like that we first carry out disturbance cancellation prior to the M-OMP iterations. At each iteration of M-OMP, the matching step is in fact equivalent to computing the 2-D delay-Doppler CCF between the residual and the reference signal. It follows that the first iteration coincides with matched filter. Different from matched filter, the highest peak of the range-Doppler map is located as a new target detected at each iteration and the location information is added into the support set. The algorithm is repeated till a fixed number of iterations or some terminating criterion is satisfied. Considering the fact that the data in practice is taken over a time window, e.g., of 1 s, which leads to a slight range-Doppler spread, and that the true delay-Doppler values may not lie exactly in the chosen delay-Doppler bins, thus a small area around the maximum of the range-Doppler map can be detected as the location of the new target that is used to update the support set.

In the second stage, the angle of the target is estimated. Note that the angle information is contained in the coefficients of the joint sparse recovery problem that has been solved in the first stage. As a result, a simple beamforming method [45] can be adopted to estimate this parameter. The range-Doppler of the target can be estimated in an iterative way, so dose the angle of the target.

The phase information contained in each channel is not affected by range-Doppler estimation. After we do the range-Doppler estimation, the phase information is contained in the L_A coefficient of the corresponding range-Doppler pairs for each target. As shown in the Fig. 2, we can pick up the values from range-Doppler 1 to range-Doppler L_A to do the beamforming for estimating the angles of targets.

To sum up, the overall algorithm is given in Algorithm 2.

Since the DOA of direct path is known, the direct path can be estimated by least squares when the received data from surveillance array $\mathbf{Y}$ is given. The target echoes can be retrieved from the received data based on disturbance cancellation, the detail is given in Section III (line 1). The range-Doppler pair of each target can be estimated based on Algorithm 1 since L_A channels share the identical support (line 2). After we do the range-Doppler estimation, the phase information is contained in L_A coefficients of corresponding range-Doppler pairs for each target. Then the angle of each target can be estimated based on the simple beamforming method (line 3). Finally, the range-Dopplers and angles of all targets can be estimated.

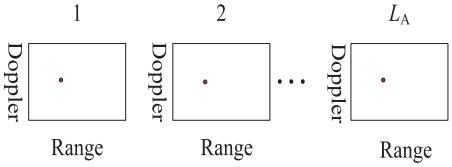

Fig. 2. Illustration of angle estimation of target.

Algorithm 2 Grid Sparse Method With Known Direct Path

Input: the received data from the surveillance array $\mathbf{Y}$,
Output: the range-Doppler and angle of the targets.

1. Disturbance cancellation to retrieve the target echoes from the array data;
2. Range-Doppler estimation using M-OMP by exploiting the joint sparsity among the L_A channels (see Algorithm 1);
3. Angle estimation for each target using beamforming.

V. Numerical Simulations

A. Simulation Setup

In this section, we will establish the modeling of the PBR system, including modeling of the transmitted signal, multipath and clutter echoes and the data acquisition process.

1) Modeling of the Transmitted Signal: Generally, different illuminators have substantially different characteristics which greatly affect the performance of the radar system. In fact, the bandwidth of the transmitted signal determines the range resolution of the radar system. The auto-ambiguity function (AAF) of a transmitted signal can measure the difference between the target echoes and the direct path and among echoes and affects the performances of later disturbance cancellation and target localization. Therefore, it is important to model the transmitted signal in PBR systems.

In the PBR system of this paper, a commercial frequency modulation radio station is employed as the transmitter antenna. Currently, there are 18 frequency modulation radio stations in Singapore with the frequencies from 88.3 to 100.3 MHz. While each radio station has a nominal assigned channel bandwidth of 200 kHz, a typical frequency modulation radio transmission occupies a bandwidth of about 100 kHz thus yielding a bistatic range resolution of about 3 km [38]. To simulate the frequency modulation radio signals a segment of a song is taken and then the frequency is modulated with a bandwidth of about 100 kHz. Fig. 3 plots the normalized spectra of modulating signal and frequency modulation signal that will be used for simulated scenario. It is noted that the

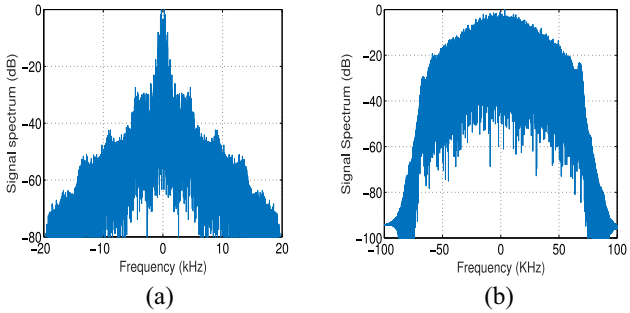

Fig. 3. Normalized spectra of (a) modulating signal and (b) frequency modulation signal used for simulated scenario.

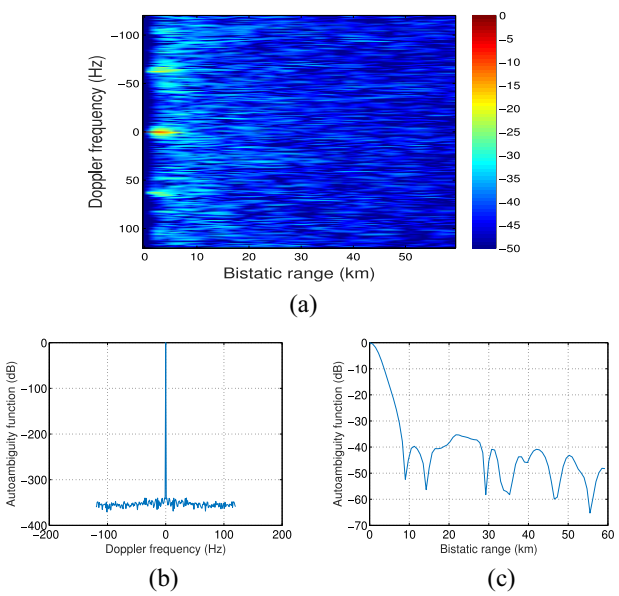

Fig. 4. Normalized 2-D AAF of frequency modulation signal used for simulated scenario. (a) 2-D representation on range-Doppler plane. (b) Zero range cut. (c) Zero Doppler cut.

spectrum of the frequency modulation signal is similar to the one in [11].

We now evaluate the self-ambiguity property of the frequency modulation signal in the range-Doppler domain. In particular, the delay-Doppler AAF of signal $s(t)$ in a time window $[0, T_0)$ is defined as

$$\xi_0(\tau, f_D) = \int_0^{T_0} s(t) \cdot s^*(t) \cdot e^{-j2\pi f_D t} dt. \tag{20}$$

With the definition in (20), the AAF measures the ambiguity level of a signal subject to a time delay τ and a Doppler shift f_D. We take the frequency modulation signal in Fig. 3 as an example. When T_0 is taken as 1 s, the AAF in range-Doppler plane is visualized in Fig. 4(a). Its zero range and zero Doppler cut are shown in Fig. 4(b) and (c), respectively. The strongest sidelobes appears around ± 65 Hz with a small range. It is shown in a further study that the peak-to-sidelobe ratio of the AAF is about 20 dB that is similar with the practical scenario [11]. Especially, the AAF is time-varying in practice and changes with the program being broadcast. However, the AAF will always exist spectrum peakings at

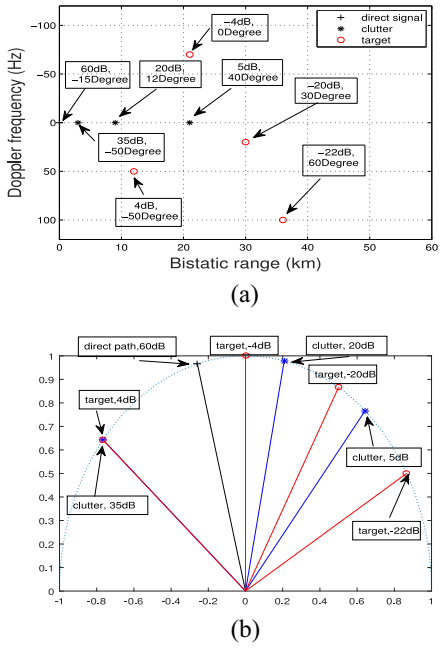

Fig. 5. Sketch of the reference scenario. In the (a) range-Doppler plane and (b) angle plane.

Doppler frequency with 0 Hz and bistatic range with 0 km as shown in Fig. 4(b) and (c), respectively.

2) Modeling of Multipath and Clutter: Given a direct signal $d(t)$, we now model the multipath and clutter, the multipath and clutter received at the surveillance antenna can be expressed as $\sum_{i=1}^{N_C} c_i d(t - \tau_{ci})$. For simplicity, we only consider the case of a single surveillance antenna while the case of an antenna array can be found in (2). Due to the low frequency of the frequency modulation signal in Singapore (88.3–100.3 MHz), multipath and clutter are represented as a set of small discrete scatterers.

3) Modeling of the Virtual Reference Signal: In proposed PBR system, the virtual reference signal serves as an estimate of the direct signal. For the sake of simplify, we model the reference signal as the direct signal plus noise

$$s_{\text{ref}}(t) = d(t) + n_{\text{ref}}(t). \tag{21}$$

Then we can generate the surveillance signals of ULA as shown in (2).

We present simulation results in this section to demonstrate the performance of the proposed algorithms. The normalized spectrum of the transmitted frequency modulation signal is the same as Fig. 3(b). Fig. 5(a) and (b) plots the reference scenario in the range-Doppler and in the angle plane, respectively. It can be seen that the direct path is from the direction of $-15°$ and has an SNR of 60 dB. Three clutters or ground scatterers from directions of $-50°$, $12°$, and $40°$ are considered with SNRs of 35, 20, and 5 dB, respectively. Four targets are present, two of which are relatively strong with SNRs of 4 and -4 dB and the other two are weaker with SNRs of -20 and -22 dB. Their bistatic ranges are also plotted. Eight antennas are implemented to form a ULA.

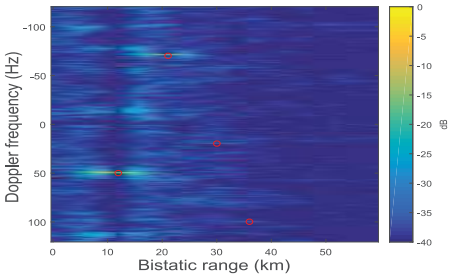

Fig. 6. Range-Doppler map of the matched filter after disturbance cancellation.

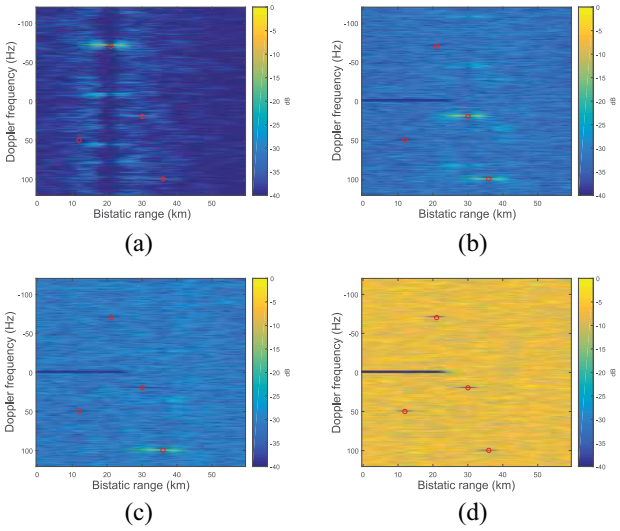

Fig. 7. Range-Doppler maps in the second to fifth iterations of M-OMP for range-Doppler estimation. (a) Second iteration. (b) Third iteration. (c) Fourth iteration. (d) Fifth iteration.

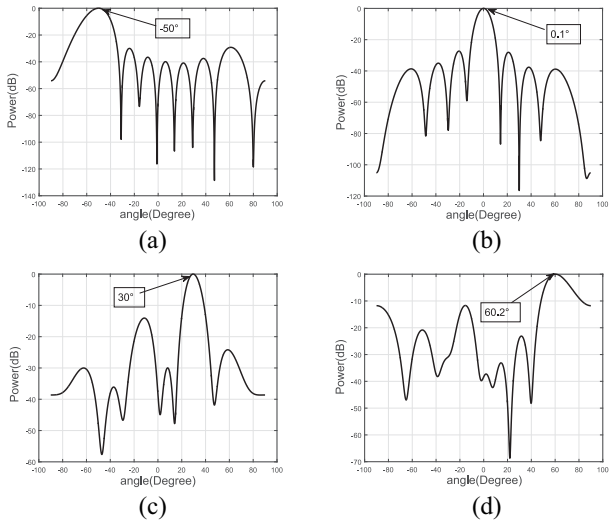

Fig. 8. Angle estimation results using beamforming after M-OMP.

Algorithm 3 Grid Sparse Method With Unknown Direct Path

Input: the received data from the surveillance array $\mathbf{Y}$,
Output: the range-Doppler and angle of the targets.

1. DOA estimation using MUSIC method given the angle of the direct path;
2. Direct path estimation using the least squares method;
3. Disturbance cancellation to retrieve the target echoes from the array data;
4. Range-Doppler estimation using M-OMP by exploiting the joint sparsity among the L_A channels (see Algorithm 1);
5. Angle estimation for each target using beamforming.

B. Angle-Range-Doppler Estimation Given Direct Path

We first consider the case when the direct path is known. After disturbance cancellation, the range-Doppler map of the conventional matched filter method can be obtained as shown in Fig. 6. It can be seen that two strong targets can be detected while the two weak targets are masked by the sidelobes of the strong ones.

We next consider the proposed compressed sensing algorithm, i.e., M-OMP, for range-Doppler estimation. It is known that the first iteration of M-OMP coincides with the matched filter. Fig. 7 presents the range-Doppler maps in the second to fifth iterations of M-OMP. It can be seen that M-OMP can detect all four targets in an iterative manner. Compared Fig. 6 with Fig. 7(a), it can be seen that the target, which is at the leftmost range-Doppler map, is detected and canceled at first, i.e., the target, which has the shortest bistatic range and the strongest SNR, is detected at first. From Figs. 6 and 7(d), it can be seen that the targets are detected from the left side of range-Doppler map to the right side of range-Doppler map, i.e., the targets are detected from the largest SNR to the smallest SNR.

Fig. 8 presents the angle estimation results using beamforming after applying M-OMP for range-Doppler estimation. It can be seen that the angles of all the targets can be accurately estimated.

C. Real Test: Direct Path-Angle-Range-Doppler Estimation

We now consider the practical case when the direct path is unknown. First of all, we need to estimate the direct path, which is crucial in the ensuing parameter estimation process. If the DOA of the direct path can be estimated, then the direct path can be estimated by using a least squares method given the array data. There have been many approaches for DOA estimation [39], e.g., conventional subspace methods like MUSIC [46], and compressed sensing (sparse) methods that can perform well in the presence of coherent sources [25], among many others. A recent class of methods known as gridless sparse methods that operate directly in the continuous domain without gridding and thus resolves the grid mismatch problem of previous grid sparse methods [30]. Since the power of direct path is much stronger than that of multipath and clutter, the conventional MUSIC algorithm can be used for DOA estimation of direct path with lower computational complexity compared with grid sparse and gridless sparse methods.

To sum up, the algorithm in the case of unknown direct path is given in five steps as follows.

When the DOA of direct path is not known, the traditional MUSIC algorithm is used for DOA estimation of direct path (line 1). The direct path can be estimated by least squares when the received data from surveillance array $\mathbf{Y}$ is given (line 2).

(a) (b)

Fig. 9. PBR system that we establish. (a) Global environment of the trial. (b) ULA.

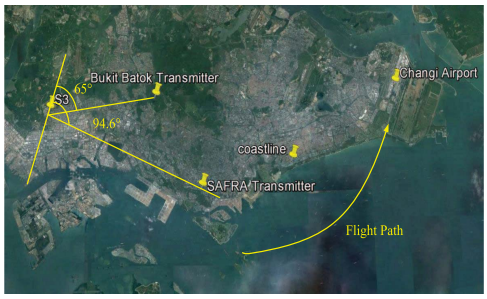

Fig. 10. Sketch map in Google earth.

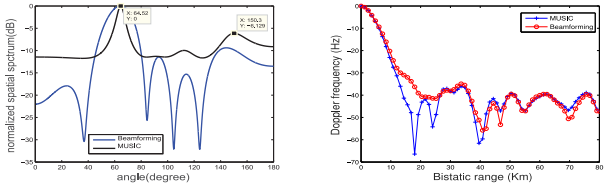

(a) (b)

Fig. 11. Direct path estimation using beamforming and MUSIC with carrier frequency 93.3 MHz of the transmitter located in Bukit Batok. Normalized (a) spatial spectrum and (b) zero Doppler cut.

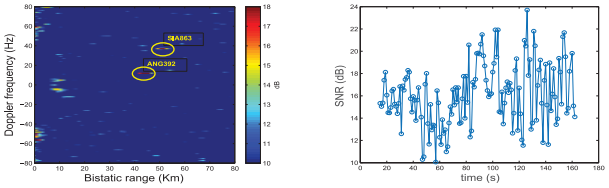

(a) (b)

Fig. 12. 2-D-CCF and SNR of target SIA863. (a) Group 137 of 90.5 MHz of 2-D CCF for detecting target SIA863. (b) Output SNR versus time for target SIA863.

Other steps are identical with Algorithm 2 (from lines 3–5). Note that the last three steps are exactly those in the case of known direct path (see Algorithm 2).

In this part, we display the PBR system that we have established and test our proposed algorithm for direct path-range-Doppler-angle estimation. The trail has been done at the roof top of S3 building in Nanyang Technological University, Singapore, and a field trial was conducted for aircraft target detection. As shown in Fig. 9, an eight-element ULA was used to receive the target echo signal. Due to the limitation of trial site, the total array length is only 8.2 m and the element spacing is 1.17 m (smaller than the half wavelength). The ULA is used to capture the spatial signal from 88 to 108 MHz. The eight-channel received signals are filtered and then digitized by a Pentek eight-channel ADC system. The ground truths of the targets can be confirmed by the ADS-B record.

As shown in Fig. 10, the ULA is displayed in S3, the transmitter that we use is located at Bukit Batok. The angle between S3 building and the Bukit Batok is 65°. The targets of flights that we need to estimate are mostly flying across the coastline, and then arrive at Changi airport. It should be noted that multiple frequencies are used for target tracking, multiple workstations or servers should be used in the hardware construction. The integrating computing will play a important role in data process, then multiple frequencies can be used for target tracking simultaneously.

1) DOA Estimation of Direct Path: First, we adopt the carrier frequency 93.3 MHz whose frequency modulation radio station located at Bukit Batok to estimate the DOA of the direct path. The normalized spatial spectrum of beamforming and MUSIC based on the received real data are plotted in Fig. 11(a). It can be seen that beamforming and MUSIC can estimate the DOA of direct path with approximated accuracy 64.52°. Moreover, the multipath/clutter may exist.

2) Direct Path Estimation: Based on the DOA estimation result of direct path and clutters, the direct path can be estimated by using least squares method. We compare the estimated performance of direct path for MUSIC and beamforming by using the normalized zero Doppler cut. Fig. 11(b) plots normalized zero Doppler cut of group 51 of carrier frequency 93.3 MHz with the transmitter located at Bukit Batok, respectively. As shown in Fig. 11(b), since the direct path estimation of MUSIC is almost identical with that of beamforming, thus the bistatic range-Doppler estimation are almost identical for MUSIC and beamforming. Thus the direct path estimation of beamforming is adopted in the following.

3) Range-Doppler Estimation: In order to improve the SNR of targets, the beamforming method is adopted. We steer the beam toward 110.00°, which is corresponding to the flight path of the targets. After disturbance cancellation, we do range-Doppler estimation based on joint sparsity among eight channels. For target SIA863 and ANG392, a 2-D CCF is given in Fig. 12(a) as an example. It can be seen that the yellow ellipse areas are two targets. In the following part, only the estimation result of target SIA863 is taken into consideration since the estimation procedures of other targets are similar as target SIA863. The output SNR versus time is given in Fig. 12(b) for target SIA863. It can be seen that the SNR is larger than 10 dB, which means that the target can be detected effectively. It should be noted that this SNR is not the maximized at each second since we just steer the beam toward 110.00°. If we track the target closely, the output SNR should be larger than this at each second.

The range and Doppler errors versus time are depicted in Fig. 13, respectively.

4) DOA Estimation: The DOA error versus time for target SIA863 using beamforming and the proposed algorithm (M-OMP) are depicted in Fig. 14. It can be seen that some outliers exist for beamforming method. Compared with the

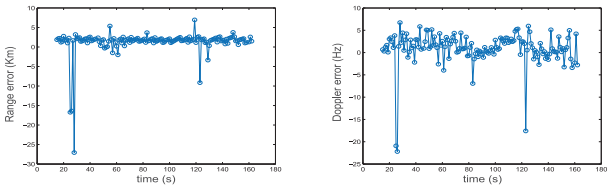

Fig. 13. Range and Doppler estimation error of target SIA863. (a) Range errors versus time. (b) Doppler errors versus time.

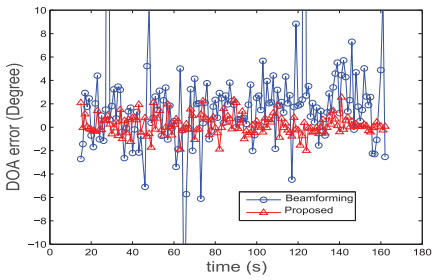

Fig. 14. DOA error versus time for target SIA863.

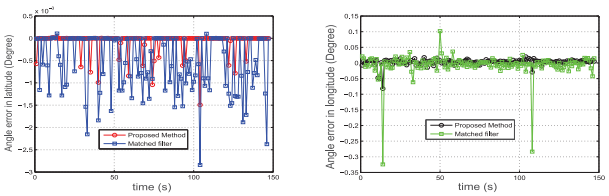

Fig. 15. Latitude and longitude errors of SIA863. (a) Latitude errors versus time. (b) Longitude errors versus time.

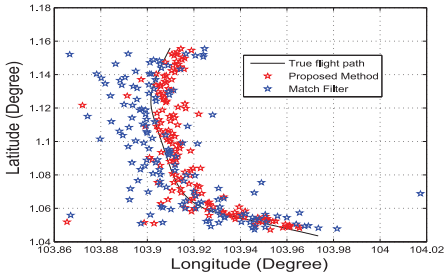

Fig. 16. Flight path for target SIA863 using matched filter and the proposed method.

beamforming method, the proposed algorithm can estimate the DOA with relatively small error. The reason can be explained as follows. For beamforming, if there is only a single target, then the CCF will be peaked at the true value of the parameter and therefore the parameter can be accurately estimated. It is also noted that there will be side lobes due to the auto-correlation of the waveform.

Now consider the case of multiple targets. The CCF will be a weighted sum of the CCFs of the targets, and the weights are determined by the power of the targets. Due to the fact that the peaks of the function can be affected by near or stronger targets, thus the peaks of the function can be different from the true parameters.

What M-OMP does is trying to minimize the effects among the targets. In particular, at the first step, it does the same thing as beamforming. But after that, it takes out the strongest one that is least likely affected by others, do cross-correlation for the rests and repeat the process. By doing so, the parameters are iteratively estimated and are expected to be more accurate.

5) Flight Path Estimation: The latitude and longitude errors for the traditional matched filter method and the proposed algorithm are plotted in Fig. 15, respectively. It can be seen that the proposed algorithm performs better than matched filter. The reason can be explained as follows. The errors of range estimation for both algorithms are identical. However, the DOA estimation accuracy using M-OMP is higher than that using beamforming, thus the proposed algorithm outperforms beamforming.

The flight paths for the matched filter method and the proposed algorithm are plotted in Fig. 16. It can be seen that the flight path using the proposed algorithm is more accurate than that using conventional matched filter method. This is because that the DOA estimation accuracy using our proposed algorithm is more accurate than that of beamforming.

VI. Discussion

The angle of target can be estimated at first. Thus the estimation accuracy of angle can be improved, since no accumulative error of range-Doppler estimation can affect the estimation accuracy of angle. However, this method has a limitation, that the number of targets cannot exceed the number of antennas. Our proposed method does not have this limitation, the tradeoff is that the estimation accuracy of angle in the proposed algorithm is lower than that of the method which estimates angle of the target at first.

For the farfield ground scatterers used to model multipath and clutter, the contributions of their angles to the surveillance signals are also exploited. But this is not fit for nearfield ground scatterers, since the propagation wavefront of the reflected signal cannot be assumed to be flat. In fact, the modeling of nearfield ground scatterers is not that important in the considered PBR system in this paper if a proper disturbance cancellation algorithm is adopted to cancel out the contributions of the direct signal and the ground scatterers.

It is interesting to note that this M-OMP algorithm from the perspective of sparse recovery is very similar to the algorithm proposed in [11]. The main difference is that the algorithm in [11] adopts a more greedy target detection scheme that attempts to detect multiple targets at each iteration. While this scheme may shorten the computational time, it more likely suffers from false alarm.

VII. Conclusion

In this paper, we have proposed compressed sensing algorithms for angle-range-Doppler estimation in intelligent tracking systems when the direct path is known and unknown, respectively. Due to the high estimation accuracy and super-resolution of gridless sparse method, we devise a simultaneous angle-range-Doppler estimation method by using atomic norm

minimization. Although the computational complexity is too high for the modern hardware, it would be possible to implement in practical scenarios in the future based on the rapid development of integrating computing. Based on the joint sparsity of multiple channels, the estimation accuracy could be improved as well compared with the method only using two reference and surveillance antennas. Numerical simulations and real test are carried out to demonstrate that the estimation accuracy of flight path of the proposed algorithm is higher than that of the traditional matched filter method. In this paper, only one surveillance array is used for parameter estimation. In the future, multiple surveillance arrays can be constructed as a surveillance network to improve the system performance, thus how to fuse the data received by different arrays and how to design the parameter estimation algorithm need to be studied in detail.

APPENDIX

It holds that $\mathbf{\Phi} = \mathbf{G}\mathbf{F}^H$, where $\mathbf{F}^H$ is the inverse 3-D discrete Fourier transform matrix with

$$\left[\mathbf{F}^H\right]_{(k,p,l)\times(k',p',l')} = \frac{1}{L_T^2 L_A} e^{i2\pi\left(\frac{p'k+k'p}{L_T}+\frac{l'l}{L_A}\right)} \tag{22}$$

and $\mathbf{G}$ is a $L_T L_A \times L_T^2 L_A$ Gabor matrix with

$$\mathbf{G}_{(k,l)\times(k',p',l')} = \hat{d}_{k-p'} e^{i2\pi\left(\frac{k'k}{L_T}+\frac{l'l}{L_A}\right)}. \tag{23}$$

To see this, we have that

$$\begin{aligned}
\mathbf{G}\mathbf{F}^H_{(k,l)\times(k',p',l')} &= \sum_{m,q=-N_T}^{N_T}\sum_{n=-N_A}^{N_A} \mathbf{G}_{(k,l)\times(m,q,n)}\left[\mathbf{F}^H\right]_{(m,q,n)\times(k',p',l')} \\
&= \frac{1}{L_T^2 L_A}\sum_{m,q=-N_T}^{N_T}\sum_{n=-N_A}^{N_A} \hat{D}_{k-q} \\
&\quad \times e^{i2\pi\left(\frac{mk}{L_T}+\frac{nl}{L_A}\right)} e^{i2\pi\left(\frac{p'm+k'q}{L_T}+\frac{l'n}{L_A}\right)} \\
&= \frac{1}{L_T^2 L_A}\sum_{q=-N_T}^{N_T} \hat{D}_{k-q} e^{i2\pi\frac{k'q}{L_T}} \sum_{m=-N_T}^{N_T} \\
&\quad e^{i2\pi\frac{(k+p')m}{L_T}} \sum_{n=-N_A}^{N_A} e^{i2\pi\frac{(l+l')n}{L_T}} \\
&= \mathbf{\Phi}_{(k,l)\times(k',p',l')}.
\end{aligned} \tag{24}$$

To make it clearer, let $\mathbf{F}_A^H$ be the (inverse) 1-D discrete Fourier transform matrix (regarding the third dimension) and $\mathbf{F}_T^H$ be the (inverse) 2-D discrete Fourier transform matrix (regarding the first two dimensions). Moreover, let $\mathbf{G}_T$ and $\mathbf{\Phi}_T$ be the Gabor matrix and the sensing matrix (regarding the first two dimensions), respectively. Then, it holds that $\mathbf{F}^H = \mathbf{F}_A^H \otimes \mathbf{F}_T^H$ and $\mathbf{G} = \mathbf{L}_A\mathbf{F}_A^H \otimes \mathbf{G}_T$. As a result

$$\mathbf{\Phi} = \mathbf{G}\mathbf{F}^H = \mathbf{L}_A\mathbf{F}_A^{2H} \otimes \mathbf{G}_T\mathbf{F}_T^H = \mathbf{E} \otimes \mathbf{\Phi}_T \tag{25}$$

where $\mathbf{E}$ is the row-reverse matrix obtained by reversely sorting the rows of the identity matrix and $\otimes$ is Kroneker product between two matrices.

REFERENCES

[1] A. Zanella, N. Bui, A. Castellani, L. Vangelista, and M. Zorzi, "Internet of Things for smart cities," *IEEE Internet Things J.*, vol. 1, no. 1, pp. 22–32, Feb. 2014.

[2] M. Chiang and T. Zhang, "Fog and IoT: An overview of research opportunities," *IEEE Internet Things J.*, vol. 3, no. 6, pp. 854–864, Dec. 2016.

[3] D. Li, N. Zhou, J. Wan, Z. Zhai, and A. V. Vasilakos, "Towards a model-integrated computing paradigm for reconfigurable motion control system," in *Proc. IEEE 14th Int. Conf. Ind. Informat. (INDIN)*, Poitiers, France, Jul. 2016, pp. 756–761.

[4] J. Jin, J. Gubbi, S. Marusic, and M. Palaniswami, "An information framework for creating a smart city through Internet of Things," *IEEE Internet Things J.*, vol. 1, no. 2, pp. 112–121, Apr. 2014.

[5] D. A. Reed and J. Dongarra, "Exascale computing and big data," *Commun. ACM*, vol. 58, no. 7, pp. 56–68, Jul. 2015.

[6] C. Berdanier, M. Wicks, C. Baker, and Z. Wu, "Phase based 2D passive source localisation using receiver networks," *Proc. Inst. Elect. Eng.—Radar Sonar Navig.*, vol. 11, no. 1, pp. 2–10, Jan. 2017.

[7] Q. Wu, Y. D. Zhang, M. G. Amin, and B. Himed, "Space—Time adaptive processing and motion parameter estimation in multistatic passive radar using sparse Bayesian learning," *IEEE Trans. Geosci. Remote Sens.*, vol. 54, no. 2, pp. 944–957, Feb. 2016.

[8] Q. He, J. Hu, R. S. Blum, and Y. Wu, "Generalized Cramér–Rao bound for joint estimation of target position and velocity for active and passive radar networks," *IEEE Trans. Signal Process.*, vol. 64, no. 8, pp. 2078–2089, Apr. 2014.

[9] Y. Liu, X. Wan, H. Tang, J. Yi, Y. Cheng, and X. Zhang, "Digital television based passive bistatic radar system for drone detection," in *Proc. IEEE Radar Conf.*, May 2017, pp. 1493–1497.

[10] P. Stinco, M. S. Greco, F. Gini, and B. Himed, "IEEE 802.22 passive radars: Multistatic detection and velocity profiler," *IEEE Trans. Aerosp. Electron. Syst.*, vol. 52, no. 5, pp. 2298–2313, Oct. 2016.

[11] F. Colone, C. Palmarini, T. Martelli, and E. Tilli, "Sliding extensive cancellation algorithm for disturbance removal in passive radar," *IEEE Trans. Aerosp. Electron. Syst.*, vol. 52, no. 3, pp. 1309–1326, Jun. 2016.

[12] H. Sun, D. K. P. Tan, Y. Lu, and M. Lesturgie, "Applications of passive surveillance radar system using cell phone base station illuminators," *IEEE Aerosp. Electron. Syst. Mag.*, vol. 25, no. 3, pp. 10–18, Mar. 2010.

[13] J. E. Palmer, H. A. Harms, S. J. Searle, and L. M. Davis, "DVB-T passive radar signal processing," *IEEE Trans. Signal Process.*, vol. 61, no. 8, pp. 2116–2126, Apr. 2013.

[14] K. S. Bialkowski, I. V. L. Clarkson, and S. D. Howard, "Generalized canonical correlation for passive multistatic radar detection," in *Proc. IEEE Stat. Signal Process. Workshop (SSP)*, Nice, France, Jun. 2011, pp. 417–420.

[15] D. E. Hack, L. K. Patton, B. Himed, and M. A. Saville "Detection in passive MIMO radar networks," *IEEE Trans. Signal Process.*, vol. 62, no. 11, pp. 2999–3012, Jun. 2014.

[16] G. Cui, J. Liu, H. Li, and B. Himedb, "Signal detection with noisy reference for passive sensing," *Signal Process.*, vol. 108, pp. 389–399, Mar. 2015.

[17] J. Liu, H. Li, and B. Himed, "On the performance of the cross-correlation detector for passive radar applications," *Signal Process.*, vol. 113, pp. 32–37, Aug. 2015.

[18] L. Wang and B. Yazici, "Passive imaging of moving targets using sparse distributed apertures," *SIAM J. Imag. Sci.*, vol. 5, no. 3, pp. 769–808, 2012.

[19] H. Wang, Z. Zhang, Y. Li, and Z. Feng, "Improved main-beam nulling through single switchable displaced element for small scale adaptive array," *IEEE Trans. Antennas Propag.*, vol. 62, no. 5, pp. 2522–2530, May 2014.

[20] R. Tao, H. Z. Wu, and T. Shan, "Direct-path suppression by spatial filtering in digital television terrestrial broadcasting-based passive radar," *IET Radar, Sonar Navig.*, vol. 4, no. 6, pp. 791–805, Dec. 2010.

[21] F. Colone *et al.*, "Space-time constant modulus algorithm for multipath removal on the reference signal exploited by passive bistatic radar," *IET Radar, Sonar Navig.*, vol. 3, no. 3, pp. 253–264, Jun. 2009.

[22] X. Zhang, H. Li, J. Liu, and B. Himed, "Joint delay and Doppler estimation for passive sensing with direct-path interference," *IEEE Trans. Signal Process.*, vol. 64, no. 3, pp. 630–640, Feb. 2016.

[23] D. L. Donoho, "Compressed sensing," *IEEE Trans. Inf. Theory*, vol. 52, no. 4, pp. 1289–1306, Apr. 2006.

[24] E. J. Candès and T. Tao, "Near-optimal signal recovery from random projections: Universal encoding strategies?" *IEEE Trans. Inf. Theory*, vol. 52, no. 12, pp. 5406–5425, Dec. 2006.

[25] L. Wan, G. Han, L. Shu, S. Chan, and N. Feng, "PD source diagnosis and localization in industrial high-voltage insulation system via multimodal joint sparse representation," *IEEE Trans. Ind. Electron.*, vol. 63, no. 4, pp. 2506–2516, Apr. 2016.
[26] Y. Chi, L. L. Scharf, A. Pezeshki, and A. R. Calderbank, "Sensitivity to basis mismatch in compressed sensing," *IEEE Trans. Signal Process.*, vol. 59, no. 5, pp. 2182–2195, May 2011.
[27] V. Chandrasekaran, B. Recht, P. A. Parrilo, and A. S. Willsky, "The convex geometry of linear inverse problems," *Found. Comput. Math.*, vol. 12, no. 6, pp. 805–849, Dec. 2012.
[28] G. Tang, B. N. Bhaskar, P. Shah, and B. Recht, "Compressed sensing off the grid," *IEEE Trans. Inf. Theory*, vol. 59, no. 11, pp. 7465–7490, Nov. 2013.
[29] B. N. Bhaskar, G. Tang, and B. Recht, "Atomic norm denoising with applications to line spectral estimation," *IEEE Trans. Signal Process.*, vol. 61, no. 23, pp. 5987–5999, Dec. 2013.
[30] Z. Yang and L. Xie, "Enhancing sparsity and resolution via reweighted atomic norm minimization," *IEEE Trans. Signal Process.*, vol. 64, no. 4, pp. 995–1006, Feb. 2016.
[31] F. Zeng, C. Li, and Z. Tian, "Distributed compressive spectrum sensing in cooperative multihop cognitive networks," *IEEE J. Sel. Topics Signal Process.*, vol. 5, no. 1, pp. 37–48, Feb. 2011.
[32] J. Chen and X. Huo, "Theoretical results on sparse representations of multiple-measurement vectors," *IEEE Trans. Signal Process.*, vol. 54, no. 12, pp. 4634–4643, Dec. 2006.
[33] L. Zhang, B. Yang, and M. Luo, "Joint delay and doppler shift estimation for multiple targets using exponential ambiguity function," *IEEE Trans. Signal Process.*, vol. 65, no. 8, pp. 2151–2163, Apr. 2017.
[34] L. Zheng and X. Wang, "Super-resolution delay-Doppler estimation for OFDM passive radar," *IEEE Trans. Signal Process.*, vol. 65, no. 9, pp. 2197–2210, May 2017.
[35] Y. Yu, A. P. Petropulu, and H. V. Poor, "Reduced complexity angle-Doppler-range estimation for MIMO radar that employs compressive sensing," in *Proc. Asilomar Conf. Signals Syst. Comput.*, Pacific Grove, CA, USA, Nov. 2009, pp. 1–4.
[36] Y. Yu, A. P. Petropulu, and H. V. Poor, "MIMO radar using compressive sampling," *IEEE J. Sel. Topics Signal Process.*, vol. 4, no. 1, pp. 146–163, Feb. 2010.
[37] Y. Yu, A. P. Petropulu, and H. V. Poor, "CSSF MIMO RADAR: Compressive-sensing and step-frequency based MIMO radar," *IEEE Trans. Aerosp. Electron. Syst.*, vol. 48, no. 2, pp. 1490–1504, Apr. 2012.
[38] P. E. Howland, H. D. Griffiths, and C. J. Baker, "Passive bistatic radar systems," in *Bistatic Radar: Emerging Technology*. Chichester, U.K.: Wiley, 2008, p. 394.
[39] L. Wan, G. Han, L. Shu, S. Chan, and T. Zhu, "The application of DOA estimation approach in patient tracking systems with high patient density," *IEEE Trans. Ind. Informat.*, vol. 12, no. 6, pp. 2353–2364, Dec. 2016.
[40] P. Stoica and R. L. Moses, *Spectral Analysis of Signals*. Upper Saddle River, NJ, USA: Prentice-Hall, 2005.
[41] H. Bolvardi, M. Derakhtian, and A. Sheikhi, "Reduced complexity generalised likelihood ratio detector for digital video broadcasting terrestrial-based passive radar," *IET Radar, Sonar Navig.*, vol. 9, no. 8, pp. 1021–1029, Oct. 2015.
[42] R. Cardinali, F. Colone, C. Ferretti, and P. Lombardo, "Comparison of clutter and multipath cancellation techniques for passive radar," in *Proc. IEEE Radar Conf.*, Boston, MA, USA, Apr. 2007, pp. 469–474.
[43] F. Colone, R. Cardinali, and P. Lombardo, "Cancellation of clutter and multipath in passive radar using a sequential approach," in *Proc. IEEE Radar Conf.*, Verona, NY, USA, Apr. 2006, pp. 24–27.
[44] R. Heckel. (2016). *Super-Resolution MIMO Radar*. [Online]. Available: http://arxiv.org/abs/1605.03230
[45] L. Wan *et al.*, "DOA estimation for coherently distributed sources considering circular and noncircular signals in massive MIMO systems," *IEEE Syst. J.*, vol. 11, no. 1, pp. 41–49, Mar. 2017.
[46] P. Rocca, M. A. Hannan, M. Salucci, and A. Massa, "Single-snapshot DoA estimation in array antennas with mutual coupling through a multiscaling BCS strategy," *IEEE Trans. Antennas Propag.*, vol. 65, no. 6, pp. 3203–3213, Jun. 2017.

Liangtian Wan (M'15) received the B.S. and Ph.D. degrees from the College of Information and Communication Engineering, Harbin Engineering University, Harbin, China, in 2011 and 2015, respectively.

From 2015 to 2017, he was a Research Fellow with the School of Electrical and Electrical Engineering, Nanyang Technological University, Singapore. He is currently an Associate Professor with the School of Software, Dalian University of Technology, Dalian, China. He has authored over 30 papers published in related international conference proceedings and journals. His current research interests include social network analysis and mining, big data, array signal processing, wireless sensor networks, and compressive sensing.

Dr. Wan has been serving as an Associate Editor for IEEE ACCESS and the *Journal of Information Processing Systems*.

Xiangjie Kong (M'13–SM'17) received the Ph.D. degree from Zhejiang University, Hangzhou, China, in 2009.

He is currently an Associate Professor with the School of Software, Dalian University of Technology, Dalian, China. He has authored or co-authored over 50 scientific papers in international journals and conferences, including the IEEE TRANSACTIONS ON INDUSTRIAL INFORMATICS, *IEEE Communications Magazine*, the IEEE TRANSACTIONS ON SYSTEMS, MAN, AND CYBERNETICS: SYSTEMS, *WWWJ, FGCS, JNCA*, *Ad Hoc Networks*, and WWW. His current research interests include big data, mobile computing, and computational social science.

Dr. Kong has served as a Guest Editor for several international journals, and the Workshop Chair or a PC member for a number of conferences. He is a Senior Member of the CCF and a member of the ACM.

Feng Xia (M'07–SM'12) received the B.Sc. and Ph.D. degrees from Zhejiang University, Hangzhou, China.

He is currently a Full Professor with the School of Software, Dalian University of Technology, Dalian, China. He has authored or co-authored 2 books and over 200 scientific papers in international journals and conferences. His current research interests include computational social science, network science, data science, and mobile social networks.

Dr. Xia has been a Guest Editor of several international journals. He has served as the General Chair, the PC Chair, the Workshop Chair, the Publicity Chair, or as a PC member for a number of conferences. He is a Senior Member of the ACM.